

InP-Based Monolithic Integration Technologies for 100/200 Gb/s Pluggable Coherent Transceivers

Hideki YAGI^{†,††a)}, Yoshihiro YONEDA^{††}, Members, Mitsuru EKAWA[†], Nonmember, and Hajime SHOJI[†], Member

SUMMARY This paper reports dual-polarization In-phase and Quadrature (DP-IQ) modulators and photodetectors integrated with the 90° hybrid using InP-based monolithic integration technologies for 100/200 Gb/s coherent transmission. The DP-IQ modulator was monolithically integrated with the Mach-Zehnder modulator array consisting of deep-ridge waveguides formed through dry etching and benzocyclobutene planarization processes. This DP-IQ modulator exhibited the low half-wavelength voltage ($V_{\pi} = 1.5$ V) and the wide 3-dB bandwidth ($f_{3dB} > 28$ GHz). The photodetector monolithically integrated with the 90° hybrid consisting of multimode interference structures was realized by the butt-joint regrowth. A responsivity including total loss of 7.9 dB in the waveguide was as high as 0.155 A/W at a wavelength of 1550 nm, and responsivity imbalance of the In-phase and Quadrature channels was less than ± 0.5 dB over the C-band. In addition, the low dark current (less than 500 pA up to 85°C @ -3.0 V) and the stable operation in the accelerated aging test (test condition: -5 V at 175°C) over 5,000 h were successfully achieved for the p-i-n-photodiode array with a buried heterostructure formed through the selective embedding regrowth. Finally, a receiver responsivity including intrinsic loss of 3 dB in the polarization beam splitter was higher than 0.070 A/W at a wavelength of 1550 nm through the integration of the spot-size converter, and demodulation of 128 Gb/s DP-QPSK and 224 Gb/s DP-16QAM modulated signals was demonstrated for the compact coherent receiver using this photodetector integrated with the 90° hybrid. Therefore, we indicated that these InP-based monolithically integrated photonic devices are very useful for 100/200 Gb/s pluggable coherent transceivers.

key words: coherent transmission, InP, DP-IQ modulator, 90° hybrid, p-i-n photodiode

1. Introduction

Optical transmission systems with a 100 Gb/s channel rate in the wavelength division multiplexing (WDM) are very attractive to cope with the significant growth of data traffic. The coherent transmission technology using digital signal processing (DSP) for multi-level modulation formats, such as quadrature phase-shift keying (QPSK) and quadrature amplitude modulation (QAM) has been widely applied to 100 Gb/s long-haul networks, since it yields a high receiver sensitivity and high resilience to linear impairments, such as chromatic dispersion and polarization mode dispersion [1]–[4]. Currently, this transmission technology has been applied to not only long-haul networks but also metro networks. As a result, high port density with downsizing of optical components is essential for cost-sensitive metro ap-

plications, and pluggable transceivers with a smaller footprint and lower power dissipation, like a 100 Gb/s form-factor pluggable (CFP) transceiver are strongly required.

Compact and low driving voltage multi-level modulators and downsizing of a 90° hybrid waveguide for receivers have been studied through various approaches, such as the silica-based planar lightwave circuit which has been widely used for passive waveguides, Silicon-photonics and InP-based monolithic integration technologies [5]–[11]. InP-based monolithic integration technologies have numerous advantages over other approaches, since photonic devices using these technologies, like dual-polarization In-phase and Quadrature (DP-IQ) modulators and photodetectors integrated with a 90° hybrid in addition to tunable lasers have contributed to downsizing and low power dissipation of modules [12]–[15]. In addition, they can allow the elimination of complicated alignments in the assembly process, resulting in low production costs and stabilization of module performance with mature process technologies [15], [16].

In this paper, we report InP-based monolithically integrated photonic devices for 100/200 Gb/s pluggable coherent transceivers. The outline of this paper is as follows. Section 2 presents the fabrication process and properties of the DP-IQ modulator. The fabrication process and properties of the photodetector integrated with the 90° hybrid are discussed in Sect. 3. Section 3 also includes performance of the compact coherent receiver using this photodetector.

2. DP-IQ Modulators

2.1 Device Design

The completed InP-based dual-polarization In-phase (X/I & Y/I channels) and Quadrature (X/Q & Y/Q channels) modulator was monolithically integrated with four Mach-Zehnder modulators (MZMs) as shown in Fig. 1. The chip size was 11 mm × 2.8 mm. An AlGaInAs multiple-quantum-well (MQW) structure which offers higher modulation efficiency and smaller loss variation at high bias voltage compared with a GaInAsP MQW structure owing to larger conduction band offset was adopted as the undoped core layer. An undoped InP layer was also inserted between core and p-doped InP cladding layers for the reduction of propagation loss in waveguides. In order to reduce parasitic capacitance in MZMs, deep-ridge waveguide stripes were planarized using the benzocyclobutene (BCB) polymer. This structure con-

Manuscript received June 14, 2016.

[†]The authors are with Transmission Devices Laboratory, Sumitomo Electric Industries, Ltd., Yokohama-shi, 244–8588 Japan.

^{††}The authors are with Sumitomo Electric Device Innovations, Inc., Yokohama-shi, 244–0845 Japan.

a) E-mail: yagi-hideki@sei.co.jp

DOI: 10.1587/transele.E100.C.179

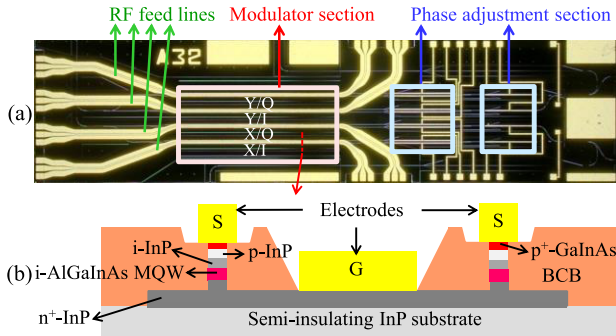


Fig. 1 (a) Photomicrograph and (b) schematic cross-sectional view of the InP-based DP-IQ modulator.

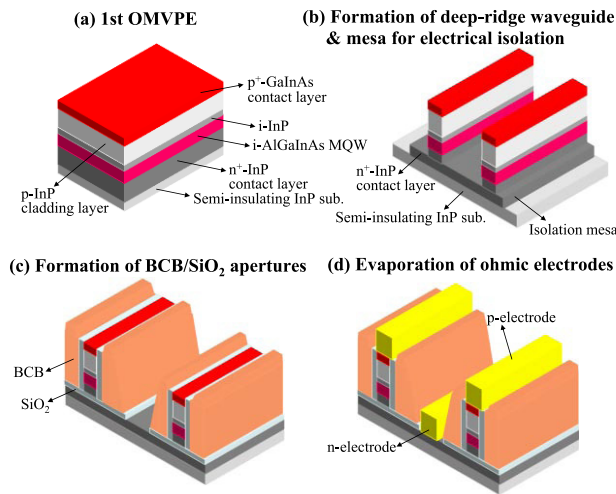


Fig. 2 Fabrication process of the InP-based DP-IQ modulator.

tributes to a wide-bandwidth characteristic enabling high-bit-rate operation [17], [18]. Each MZM is driven by a differential signal to reduce power dissipation of modulator driver ICs, and the differential characteristic impedance of the modulator section was designed to be $90\text{-}\Omega$ for RF feed lines and MZM electrodes.

2.2 Fabrication Process

Figure 2 shows the fabrication process of the InP-based DP-IQ modulator. At first, the undoped core layer consisting of the AlGaInAs MQW structure was prepared on a semi-insulating 3-inch InP wafer by an organometallic vapor-phase-epitaxial (OMVPE) growth [Fig. 2 (a)]. Deep-ridge waveguide stripes and mesas for electrical isolation of MZMs were formed by standard optical i-line stepper lithography and reactive ion etching (RIE) techniques, respectively [Fig. 2 (b)]. Then, the deposition of SiO_2 and coating of BCB polymers were carried out on surfaces of MZMs. In order to suppress electrical propagation loss at crossings of electrical transmission lines and ridge waveguides, MZMs were planarized with a relatively thick BCB polymer. BCB/ SiO_2 apertures for p- and n-side ohmic contacts were formed through photolithography and RIE tech-

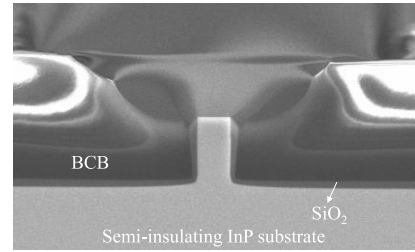


Fig. 3 Cross-sectional scanning electron microscope image after formation of the BCB/ SiO_2 aperture for the p-side ohmic contact.

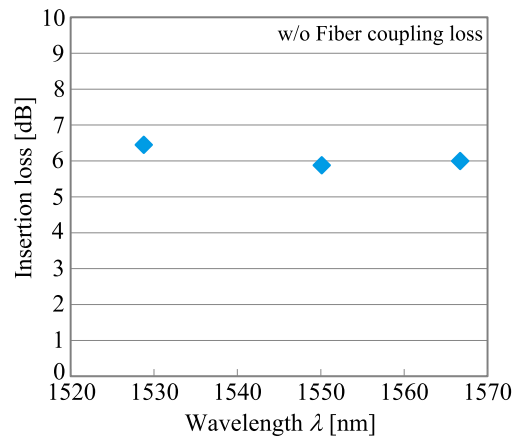


Fig. 4 Wavelength dependence of insertion loss without fiber coupling loss for the InP-based DP-IQ modulator.

niques as shown in Fig. 3 [Fig. 2 (c)] [17].

Then, electrodes were evaporated for p- and n-side ohmic contacts, followed by anti-reflection (AR) coatings on the optical input/output facets [Fig. 2 (d)].

2.3 Device Performance

Figure 4 shows wavelength dependence of insertion loss for the fabricated DP-IQ modulator. Insertion loss including intrinsic loss of QPSK (3 dB) without fiber coupling loss (2.5 dB/facet) was estimated to be less than 7 dB over the C-band. Additionally, propagation loss for the waveguide width of $1.4\text{ }\mu\text{m}$ was as low as 0.25 dB/mm over the C-band. This result indicates that scattering loss at sidewalls of fabricated deep-ridge waveguides in both straight and bending regions was suppressed by optimizing the RIE condition for formation of deep-ridge waveguides.

Figure 5 (a) shows a typical DC extinction characteristic for one MZM over the C-band. The horizontal axis indicates differential voltage superimposed at bias voltage. The bias voltage was adjusted to keep the same modulation efficiency over the C-band. The half-wavelength voltage (V_π) was as low as 1.5 V. The DC extinction ratio (ER) was larger than 25 dB over the C-band. Figure 5 (b) shows the small-signal frequency response at a wavelength of 1550 nm for the DP-IQ modulator. A 3-dB electrical/optical bandwidth of 28 GHz was obtained for all of four MZMs, and input

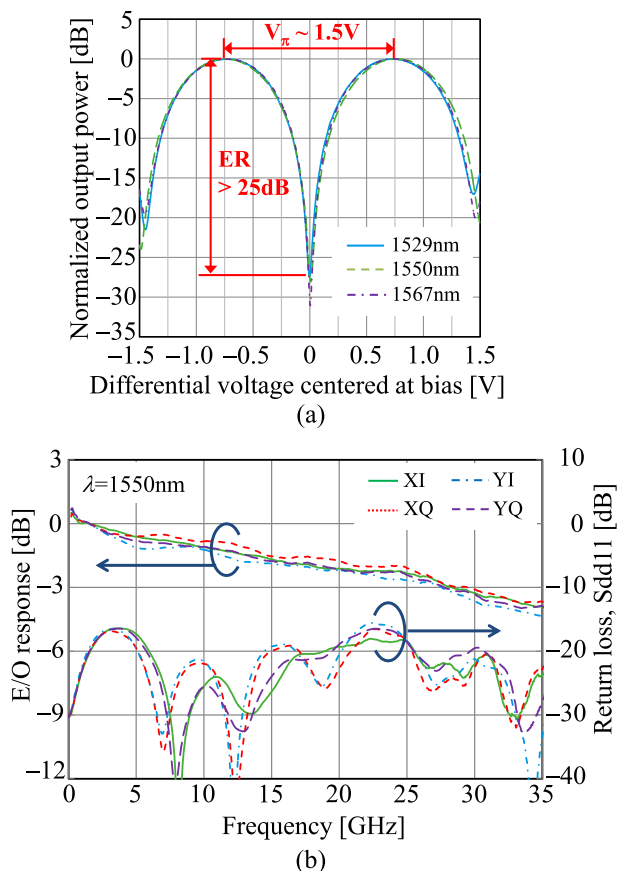


Fig. 5 (a) DC extinction characteristic over the C-band of one MZM and (b) small-signal frequency response at a wavelength of 1550 nm for the InP-based DP-IQ modulator consisting of the MZM array.

return loss was less than -16 dB up to 35 GHz. Hence, these results which are sufficient for 100 Gb/s DP-QPSK and 200 Gb/s DP-16QAM operation were successfully achieved in the InP-based DP-IQ modulator.

3. Photodetectors Integrated with the 90° Hybrid

3.1 Device Design

Figure 6 shows (a) the photomicrograph, (b) the schematic diagram of the 90° hybrid and (c) cross-sectional scanning electron microscope images of spot-size converter (SSC), 90° hybrid and p-i-n-photodiode sections for the InP-based photodetector monolithically integrated with the 90° hybrid. The chip size was $4.1 \text{ mm} \times 1.6 \text{ mm}$. The 90° hybrid has the 2×4 multimode interference structure (MMI) working as a 180° hybrid for in-phase relation, the 45° phase shifter and 2×2 MMI working for quadrature phase relation. Accordingly, the output channels from the 90° hybrid can be directly connected with the photodiode array without waveguide intersections which cause excess loss, that is, the In-phase channels (CH-1 and CH-2) and the Quadrature channels (CH-3 and CH-4) are not spatially separated in this 90° hybrid design [19], [20]. The asymmetric waveguide

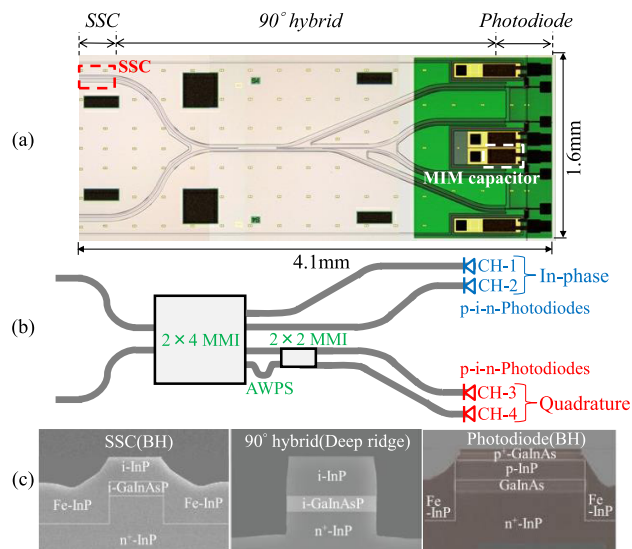


Fig. 6 (a) Photomicrograph, (b) schematic diagram of the 90° hybrid and (c) cross-sectional scanning electron microscope images of SSC, 90° hybrid and photodiode sections for the InP-based photodetector monolithically integrated with the 90° hybrid.

phase shifter (AWPS) employing the difference of the optical path length was adopted as the 45° phase shifter, because this structure with the delayed waveguide in one side of the Quadrature channels can afford the phase shift without precise control of the waveguide width as shown in Fig. 6 (b). As a result, AWPS has larger tolerance in waveguide width variation compared with the phase shifter employing the difference of the waveguide width [21]. Furthermore, in order to suppress frequency dependence of the common mode rejection ratio (CMRR), the waveguide layout of the In-phase and Quadrature channels was designed by considering the reduction of skew in the 90° hybrid, and skew was almost negligible in this 90° hybrid layout, which was estimated to be less than 0.5 ps.

A buried heterostructure (BH) was selectively formed in photodiode sections to reduce the dark current and in SSC sections for achieving high optical coupling efficiency between the polarization beam splitter (PBS) and the 90° hybrid through the selective embedding regrowth technique. The SSC core width was optimized to acquire optical coupling efficiency of more than 90% for an optical field consisting of the parallel Gaussian beam in horizontal and vertical directions, which corresponds to the mode field diameter (MFD) of $1.8 \mu\text{m}$ from the optical configuration with lens coupling. This MFD was optimized with vertical MFD which is restricted by the thickness of the upper InP cladding layer for the reduction of wavelength dependence of optical loss and for precise phase control in the 90° hybrid consisting of MMIs [22].

Moreover, capacitors consisting of metal-insulator-metal (MIM) were monolithically integrated with the photodiode array for downsizing of receiver modules [23].

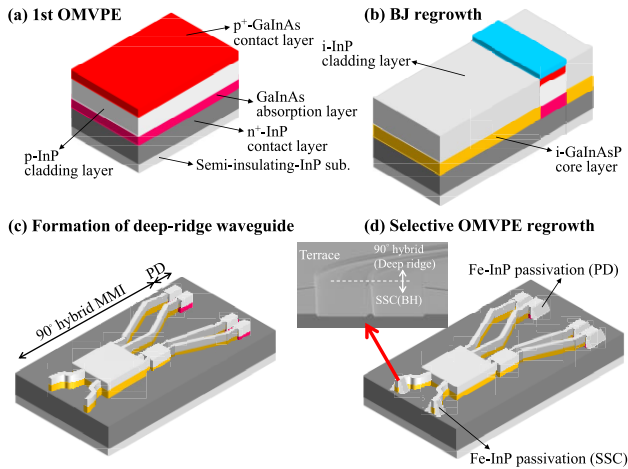


Fig. 7 Fabrication process of the InP-based photodetector monolithically integrated with the 90° hybrid. The scanning electron microscope image of the SSC section is also indicated in the inset of Fig. 7 (d).

3.2 Fabrication Process

Figure 7 shows the fabrication process of the InP-based photodetector integrated with the 90° hybrid [22]. A p-i-n-photodiode structure with a GaInAs absorption layer was prepared on a semi-insulating 3-inch InP wafer by OMVPE growth [Fig. 7 (a)]. The waveguide section with the GaInAsP core layer and the photodiode section were combined using the butt-joint (BJ) regrowth process [Fig. 7 (b)]. Deep-ridge waveguide stripes for SSC, 90° hybrid and photodiode sections were simultaneously formed by standard optical i-line stepper lithography and RIE techniques [Fig. 7 (c)].

BH layers were simultaneously formed in photodiode and SSC sections using selective OMVPE regrowth techniques [Fig. 7 (d)] [22]. As can be seen in Fig. 6 (c), although relatively thin InP passivation was adopted in the photodiode section to suppress parasitic capacitance for a high-speed response, thicker InP passivation was formed in the SSC section to obtain target MFD using the wider selective regrowth mask on the terrace part in the side of the SSC waveguide compared with that of the photodiode section. As a result, the p-i-n-photodiode array monolithically integrated with the 90° hybrid and SSC was realized through the simple fabrication process with the selective regrowth technique.

3.3 Device Performance

Figure 8 (a) shows wavelength dependence of the responsivity for the photodetector integrated with the 90° hybrid. The responsivity at a wavelength of 1550 nm including hybrid splitting loss of 6.0 dB, propagation loss of 0.4 dB and fiber coupling loss of 1.5 dB was as high as 0.155 A/W in the average of all channels. This high responsivity was achieved through high optical coupling efficiency with the BJ struc-

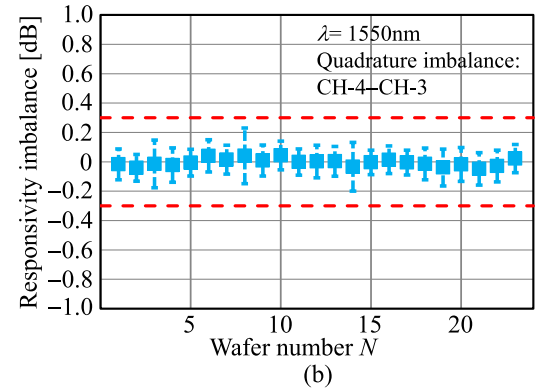
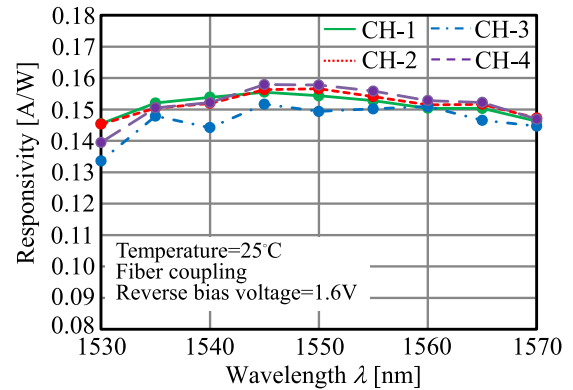


Fig. 8 (a) Wavelength dependence of responsivity and (b) reproducibility of responsivity imbalance for the Quadrature channels at a wavelength of 1550 nm over wafers (number of wafers: 23) for the photodetector integrated with the 90° hybrid.

ture, which was comprised of the 90° hybrid and the p-i-n-photodiode array. The typical responsivity including fiber coupling loss (w/ AR coating) of 1.5 dB was also 0.68 A/W at a wavelength of 1550 nm for the discrete photodiode (total length of photodiode and waveguide with the BJ interface sections: 0.9 mm) fabricated on the same wafer with the integrated device. From this result, we assumed that excess loss caused by the BJ regrowth process is almost negligible [24]. A change of responsivity due to wavelength dependence of optical loss for the 90° hybrid consisting of MMIs was less than 0.6 dB over the C-band. Responsivity imbalance of the In-phase and Quadrature channels was less than ± 0.5 dB over the C-band through small loss imbalance of the 90° hybrid consisting of 2×4 MMI, AWPS working as the 45° phase shifter and 2×2 MMI.

Figure 8 (b) shows reproducibility of responsivity imbalance for the Quadrature channels at a wavelength of 1550 nm over wafers (number of wafers: 23). Error bars indicate the standard deviation of each wafer. Good uniformity of less than ± 0.3 dB in responsivity imbalance of each wafer was attained, which is regarded as less than ± 0.5 dB over the C-band from wavelength dependence of the 45° phase shifter. This result indicates that stable manufacturability was achieved in the 90° hybrid consisting of 2×4 MMI, AWPS working as the 45° phase shifter and $2 \times$

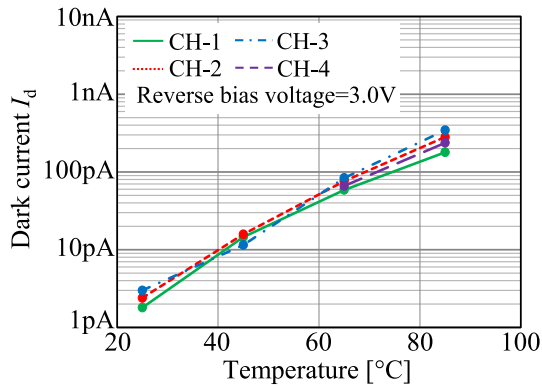


Fig. 9 Temperature dependence of the dark current for the photodetector integrated with the 90° hybrid at a reverse bias voltage of 3.0 V.

2 MMI fabricated with dry etching processes.

Figure 9 shows temperature dependence of the dark current for the photodetector integrated with the 90° hybrid at a reverse bias voltage of 3.0 V. The dark current of less than 5.0 pA was obtained at a temperature of 25°C, and the low dark current of less than 500 pA was attained even at a temperature of 85°C. This result indicates that the surface recombination at the sidewall of the deep-ridge stripe in the photodiode section was reduced through passivation effect with the InP regrowth process. Furthermore, Fe-doped InP passivation in the photodiode section is very effective compared with undoped InP passivation for the reduction of the leakage current at the interface of the deep-ridge stripe and the BH layer. Consequently, the dark current of Fe-doped InP passivation was reduced to 1/10 of undoped InP passivation [22].

The accelerated aging test for the photodetector monolithically integrated with the 90° hybrid using the above-mentioned process was carried out under a reverse bias voltage of 5 V at a high temperature of 175°C. The dark current in each channel of 11 samples under a reverse bias voltage of 3.0 V at a temperature of 25°C was evaluated in each aging time. As a result, no significant changes were observed in all channels as shown in Fig. 10, that is, the stable operation over 5,000 h was successfully achieved with InP passivation effect using the selective regrowth process. This result indicates that this InP-based monolithically integrated photonic device fabricated by the above-mentioned process has sufficient reliability for commercial applications of compact coherent receivers.

3.4 Receiver Module Performance

Figure 11 shows (a) the photograph and (b) the schematic diagram for a fabricated polarization and phase diversity intradyne coherent receiver (ICR). This receiver was comprised of a beam splitter (BS), PBS, two InP-based photodetectors monolithically integrated with the 90° hybrid and MIM capacitors for transverse electric (TE) polarized light (X-polarization) and transverse magnetic (TM) polarized light (Y-polarization) and four trans-impedance amplifiers (TIAs)

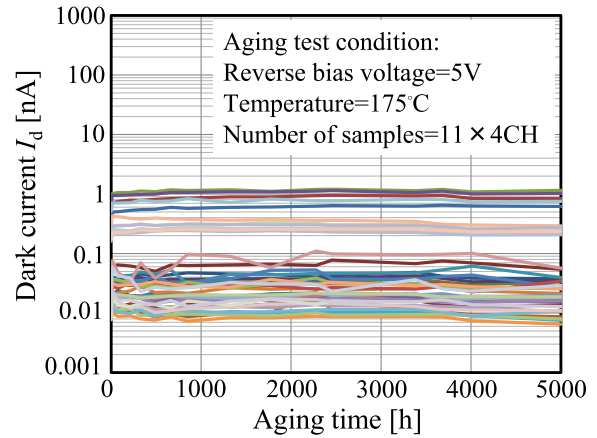
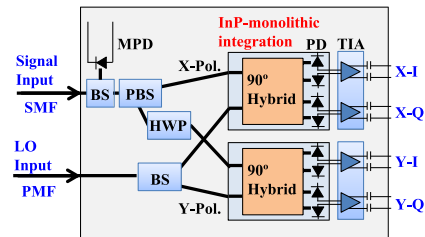


Fig. 10 Reliability test in four channels of the photodetector monolithically integrated with the 90° hybrid. The dark current in each aging time was measured under a reverse bias voltage of 3.0 V at a temperature of 25°C.



(a)



(b)

Fig. 11 (a) Photograph and (b) schematic diagram for the coherent receiver using InP-based photodetectors monolithically integrated with the 90° hybrid.

in one package [25]. The signal light with arbitrary polarization is introduced to the receiver through a single mode fiber (SMF). The signal light from SMF is coupled to the collimate lens. Then, a small portion of the signal light is split to the monitor photodiode (MPD) with BS. At PBS, the signal light is decomposed to TE polarized light and TM polarized light. The TE polarized light is coupled to the 90° hybrid for X-polarization through the lens. The TM polarized light is converted to TE polarized light with the half-wave plate (HWP). Then, this TE polarized light is coupled to the 90° hybrid for Y-polarization through the lens.

The local oscillator (LO) light is also introduced to the receiver through a polarization maintaining fiber (PMF). The LO light from PMF is coupled to the collimate lens, and this light is split with BS. Finally, the LO light is coupled to the 90° hybrid for X-polarization and that for Y-polarization

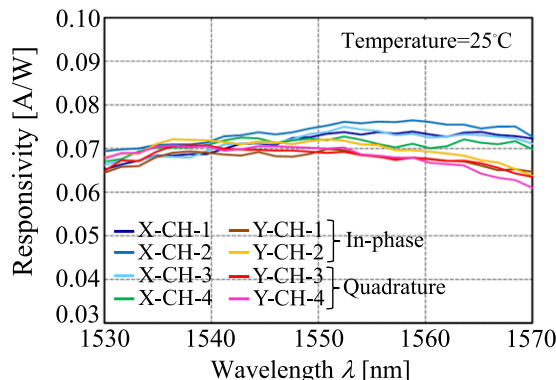


Fig. 12 Wavelength dependence of the responsivity at a temperature of 25°C for the coherent receiver using two InP-based photodetectors monolithically integrated with the 90° hybrid.

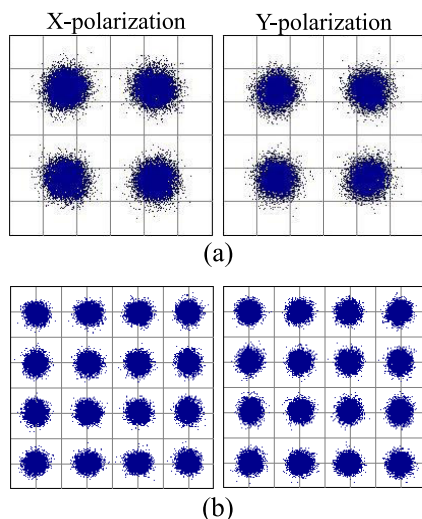


Fig. 13 Constellation diagrams with (a) 128 Gb/s DP-QPSK and (b) 224 Gb/s DP-16QAM modulated signals for the coherent receiver using InP-based photodetectors monolithically integrated with the 90° hybrid.

through the lens. The package body size was 22.7 mm × 12.0 mm × 4.6 mm, and it is small enough to install the component in 100/200 Gb/s pluggable coherent transceivers such as CFP/CFP2.

Figure 12 shows wavelength dependence of the responsivity at a temperature of 25°C for the receiver using two InP-based photodetectors monolithically integrated with the 90° hybrid and SSC. The receiver responsivity in all channels of 4 channels × 2 integrated devices was higher than 0.070 A/W at a wavelength of 1550 nm with the introduction of SSC, even though the intrinsic loss of 3 dB was caused by separation of TE polarized light and TM polarized light in PBS. Responsivity imbalance of the In-phase and Quadrature channels was also less than ±0.5 dB over the C-band, and CMRR of the In-phase and Quadrature channels was lower than -25 dB over the C-band for X-polarization and Y-polarization through small loss imbalance of the 90° hybrid.

Constellation diagrams were evaluated using 128 Gb/s

DP-QPSK and 224 Gb/s DP-16QAM modulated signals. As can be seen in Fig. 13, clear segregation among each symbol was observed at the optical-signal-to-noise-ratio (OSNR) of 20 dB and 41 dB for DP-QPSK and DP-16QAM, respectively. Hence, demodulation of 128 Gb/s DP-QPSK and 224 Gb/s DP-16QAM modulated signals was successfully demonstrated using the compact coherent receiver using InP-based photodetectors monolithically integrated with the 90° hybrid.

4. Conclusions

We demonstrated DP-IQ modulators consisting of the MZM array and photodetectors integrated with the 90° hybrid using InP-based monolithic integration technologies. The MZM array consisting of deep-ridge waveguides fabricated through dry etching and BCB planarization processes exhibited the low half-wavelength voltage ($V_{\pi} = 1.5$ V) and the wide 3-dB bandwidth ($f_{3dB} > 28$ GHz).

The photodetector monolithically integrated with the 90° hybrid consisting of MMIs by the BJ regrowth has the high responsivity (0.155 A/W at a wavelength of 1550 nm), and it was compatible with the stable dark current (> 5,000 h) with the BH layer of the photodiode section and excellent CMRR based on small loss imbalance of the 90° hybrid consisting of deep-ridge waveguides through the selective regrowth process. In addition, demodulation of 128 Gb/s DP-QPSK and 224 Gb/s DP-16QAM modulated signals was indicated as the receiver performance. Therefore, these results prove that the InP-based monolithically integrated photonic devices are very suitable for 100/200 Gb/s pluggable coherent transceivers.

References

- [1] S. Tsukamoto, D.-S. Ly-Gagnon, K. Katoh, and K. Kikuchi, "Coherent Demodulation of 40-Gbit/s Polarization-Multiplexed QPSK Signals with 16-GHz Spacing after 200-km Transmission," Proc. OFC/NFOEC 2005, Anaheim, CA, paper PDP29, pp.1-3, March 2005.
- [2] R. Noe, "Phase Noise-Tolerant Synchronous QPSK/BPSK Baseband-Type Intradynne Receiver Concept With Feedforward Carrier Recovery," IEEE J. Lightwave Technol., vol.23, no.2, pp.802-808, Feb. 2005.
- [3] G. Charlet, J. Renaudier, H. Mardoyan, P. Tran, O. Bertran Pardo, F. Verluise, M. Achouche, A. Boutin, F. Blache, J.-Y. Dupuy, and S. Bigo, "Transmission of 16.4Tbit/s Capacity over 2,550km using PDM QPSK Modulation Format and Coherent Receiver," Proc. OFC/NFOEC 2008, paper PDP3, pp.1-3, San Diego, CA, Feb. 2008.
- [4] S. Oda, T. Tanimura, T. Hoshida, C. Ohshima, H. Nakashima, Z. Tao, and J.C. Rasmussen, "112 Gb/s DP-QPSK Transmission Using a Novel Nonlinear Compensator in Digital Coherent Receiver," Proc. OFC/NFOEC 2009, San Diego, CA, paper OThR6, pp.1-3, March 2009.
- [5] H.-G. Bach, A. Matiss, C.C. Leonhardt, R. Kunkel, D. Schmidt, M. Schell, and A. Umbach, "Monolithic 90° Hybrid with Balanced PIN Photodiodes for 100 Gbit/s PM-QPSK Receiver Applications," Proc. OFC/NFOEC 2009, San Diego, CA, paper OMK5, pp.1-3, March 2009.
- [6] N. Kikuchi, Y. Shibata, K. Tsuzuki, H. Sanjoh, T. Sato, E. Yamada, T. Ishibashi, and H. Yasaka, "80-Gb/s Low-Driving-Voltage InP

- DQPSK Modulator With an n-p-i-n Structure," *IEEE Photon. Technol. Lett.*, vol.21, no.12, pp.787–789, June 2009.
- [7] Y. Painchaud, M. Pelletier, M. Poulin, F. Pelletier, C. Latrasse, G. Robidoux, S. Savard, J.-F. Gagne, V. Trudel, M.-J. Picard, P. Poulin, P. Sirois, F. D'Amours, D. Asselin, S. Paquet, C. Paquet, M. Cyr, M. Guy, M. Morsy-Osman, Q. Zhuge, X. Xu, M. Chagnon, and D.V. Plant, "Ultra-Compact Coherent Receiver Based on Hybrid Integration on Silicon," *Proc. OFC/NFOEC 2013*, paper OM2J.2, pp.1–3, Anaheim, CA, March 2013.
- [8] K. Goi, H. Kusaka, A. Oka, Y. Terada, K. Ogawa, T.-Y. Liow, X. Tu, G.-Q. Lo, and D.-L. Kwong, "DQPSK/QPSK Modulation at 40-60 Gb/s using Low-Loss Nested Silicon Mach-Zehnder Modulator," *Proc. OFC/NFOEC 2013*, Anaheim, CA, paper OW4J.4, pp.1–3, March 2013.
- [9] M. Itoh and Y. Kurata, "Heterogeneous integration of InP PDs on Silica-based PLCs," *Proc. OFC/NFOEC 2013*, Anaheim, CA, paper OTh3H.4, pp.1–3, March 2013.
- [10] C. Doerr, L. Chen, D. Vermeulen, T. Nielsen, S. Azemati, S. Stulz, G. McBrien, X.-M. Xu, B. Mikkelsen, M. Givehchi, C. Rasmussen, and S.-Y. Park, "Single-Chip Silicon Photonics 100-Gb/s Coherent Transceiver," *Proc. OFC/NFOEC 2014*, San Francisco, CA, PDP paper Th5C.1, pp.1–3, March 2014.
- [11] M. Takahashi, Y. Uchida, S. Yamasaki, J. Hasegawa, and T. Yagi, "Compact and Low-Loss Coherent Mixer Based on High Δ ZrO₂-SiO₂ PLC," *IEEE J. Lightwave Technol.*, vol.32, no.17, pp.3081–3088, Sept. 2014.
- [12] T. Kaneko, Y. Yamauchi, K. Uesaka, and H. Shoji, "A Single-Stripe Tunable Laser Operated at Constant Temperature Using Thermo-Optic Effect," *Proc. 17th Microoptics Conference (MOC '11)*, paper G-2, pp.1–2, Sendai, Japan, Oct./Nov. 2011.
- [13] N. Kono, T. Kitamura, H. Yagi, N. Itabashi, T. Tatsumi, Y. Yamauchi, K. Fujii, K. Horino, S. Yamanaka, K. Tanaka, K. Yamaji, C. Fukuda, and H. Shoji, "Compact and Low Power DP-QPSK Modulator Module with InP-Based Modulator and Driver ICs," *Proc. OFC/NFOEC 2013*, Anaheim, CA, paper OW1G.2, pp.1–3, March 2013.
- [14] R.A. Griffin, "InP-Based High-Speed Transponder," *Proc. OFC/NFOEC 2014*, San Francisco, CA, paper W3B.7, pp.1–3, March 2014.
- [15] H. Yagi, N. Inoue, R. Masuyama, T. Kikuchi, T. Katsuyama, Y. Tateiwa, K. Uesaka, Y. Yoneda, M. Takechi, and H. Shoji, "InP-Based p-i-n-Photodiode Array Integrated With 90° Hybrid Using Butt-Joint Regrowth for Compact 100 Gb/s Coherent Receiver," *IEEE J. Sel. Topics Quantum Electron.*, vol.20, no.6, pp.374–380, Nov./Dec. 2014.
- [16] V.E. Houtsma, N.G. Weimann, T.-C. Hu, R. Kopf, A. Tate, J. Frackoviak, R. Reyes, Y.-K. Chen, C.R. Doerr, L. Zhang, and D. Neilson, "Manufacturable Monolithically Integrated InP Dual-Port Coherent Receiver for 100G PDM-QPSK Applications," *Proc. OFC/NFOEC 2011*, Los Angeles, CA, paper OML2, pp.1–3, March 2011.
- [17] H. Yagi, K. Koyama, Y. Onishi, H. Yoshinaga, H. Ichikawa, N. Kaida, T. Nomaguchi, K. Hiratsuka, and K. Uesaka, "26 Gbit/s Direct Modulation of AlGaInAs/InP Lasers with Ridge-Waveguide Structure Buried by Benzocyclobutene Polymer," *Proc. The 21st Indium Phosphide and Related Materials Conference (IPRM2009)*, Newport Beach, CA, ThB1.3, pp.371–374, May 2009.
- [18] H. Yagi, T. Kitamura, N. Kono, H. Kobayashi, N. Inoue, K. Horino, D. Kimura, K. Fujii, Y. Yoneda, C. Fukuda, and H. Shoji, "Low Driving Voltage InP-Based Mach-Zehnder Modulators for Compact 128 Gb/s DP-QPSK Module," *Proc. The 10th Conference on Lasers and Electro-Optics Pacific Rim (CLEO-PR), and The 18th Opto-Electronics and Communications Conference (OECC)/ Photonics in Switching 2013 (PS2013)*, Kyoto, Japan, WK2-2, pp.1–2, July 2013.
- [19] S.-H. Jeong and K. Morito, "Novel Optical 90° Hybrid with Low Wavelength Sensitive Power Balance and Phase Deviation over 94-nm-wide Spectral Range," *Proc. European Conference and Exhibition on Optical Communication (ECOC) 2009*, paper 2.2.3, pp.1–4, Vienna, Austria, Sept. 2009.
- [20] S.-H. Jeong and K. Morito, "Compact InP-Based 90° Hybrid Using A Tapered 2×4 MMI And A 2×2 MMI Coupler," *Proc. Indium Phosphide and Related Materials (IPRM) 2010*, Kagawa, Japan, paper FrA1-4, pp.457–460, May-June 2010.
- [21] T. Okimoto, H. Yagi, R. Masuyama, K. Sakurai, Y. Nishimoto, T. Kikuchi, K. Horino, T. Watanabe, M. Ekawa, M. Takechi, and Y. Yoneda, "Small Responsivity Imbalance of InP-based p-i-n Photodiode Array Monolithically Integrated with 90° Hybrid Using Asymmetric Waveguide Phase Shifter for Coherent Detection," *Proc. Indium Phosphide and Related Materials (IPRM) 2016*, Toyama, Japan, paper MoC4-5, pp.1–2, June 2016.
- [22] H. Yagi, N. Inoue, T. Kikuchi, R. Masuyama, T. Katsuyama, Y. Tateiwa, K. Uesaka, Y. Yoneda, M. Takechi, and H. Shoji, "High receiver responsivity and low dark current of InP-based pin-photodiode array monolithically integrated with 90° hybrid and spot-size converter using selective embedding regrowth," *IEICE Electron. Express*, vol.12, no.2, pp.1–7, Jan. 2015.
- [23] R. Masuyama, H. Yagi, N. Inoue, Y. Onishi, T. Katsuyama, T. Kikuchi, Y. Yoneda, and H. Shoji, "Monolithic Integration of InP-Based Waveguide Photodiodes with MIM Capacitors for Compact Coherent Receiver," *Proc. Indium Phosphide and Related Materials (IPRM) 2013*, Kobe, Japan, paper MoD3-6, pp.1–2, May 2013.
- [24] H. Yagi, N. Inoue, R. Masuyama, T. Katsuyama, T. Kikuchi, Y. Onishi, Y. Yoneda, and H. Shoji, "High Responsivity and Wide Bandwidth Operation of InP-Based pin-Photodiode Array Monolithically Integrated with 90° Hybrid Using Butt-Joint Regrowth," *Jpn. J. Appl. Phys.*, vol.53, no.2, pp.020305-1–020305-3, Jan. 2014.
- [25] M. Takechi, Y. Tateiwa, and S. Ogita, "Compact 100G Coherent Receiver Using InP-based 90° Hybrid Integrated with Photodiodes," *Proc. European Conference and Exhibition on Optical Communication (ECOC) 2013*, paper P.2.8, pp.1–3, London, UK, Sept. 2013.



Hideki Yagi received the Ph.D. degree in physical electronics from the Tokyo Institute of Technology, Tokyo, Japan, in March 2004. During his Ph.D. study, he mainly focused on topics of long-wavelength semiconductor lasers based on low-damage and high-uniformity low-dimensional quantum structures. From 2005, he joined Transmission Devices Laboratory, Sumitomo Electric Industries, Ltd., Yokohama, Japan. His research interests are InP-based monolithic integration technologies for coherent transmission systems. Dr. Yagi was awarded the best paper award from The 10th Conference on Lasers and Electro-Optics Pacific Rim (CLEO-PR), and The 18th OptoElectronics and Communications Conference (OECC)/ Photonics in Switching 2013 (PS2013). Dr. Yagi is a member of IEICE, JSAP, and IEEE Photonics Society (Senior Member).



Yoshihiro Yoneda received the B.E. and M.E. degrees from the Nagoya Institute of Technology, Nagoya, Japan, in 1994, and 1996, respectively. In 1996, he joined Fujitsu Laboratories Ltd., Atsugi, Japan, where he has since been engaged in the research and development of high-speed photodetectors. In 2004, he joined Eudyna Devices Inc., Yamanashi/Yokohama, Japan, where he was involved in the development of optoelectronic integrated circuits (OEICs) on InP. In 2009, he joined Sumitomo Electric Industries Ltd., Yokohama, Japan. He is currently leading the development of InP-based photonic integrated devices as a group manager of Sumitomo Electric Device Innovations, Inc. Mr. Yoneda is a member of the IEICE and the IEEE Photonics/Electron Devices Societies.

He is currently leading the development of InP-based photonic integrated devices as a group manager of Sumitomo Electric Device Innovations, Inc. Mr. Yoneda is a member of the IEICE and the IEEE Photonics/Electron Devices Societies.



Mitsuru Ekawa received the B.E., M.E., and Ph.D. degrees from the Osaka University, Osaka, Japan, in 1987, 1989, and 1993, respectively. During 1989-1993, he worked at the Nagoya Institute of Technology, Nagoya, Japan, to research II-VI compound semiconductors. In 1993, he joined Fujitsu Laboratories Ltd., Atsugi, Japan, where he was engaged in research and development of OMVPE growth of III-V compound semiconductors for optical communication. In 2014, he joined Sumitomo Electric Industries, Ltd., Yokohama, Japan, where he has been engaged in development of integrated semiconductor optical devices. Dr. Ekawa is a member of JSAP.

Dr. Ekawa is a member of JSAP.



Hajime Shoji received the B.E., M.E., and Ph.D. degrees in electronic engineering from the University of Tokyo, Tokyo, Japan, in 1985, 1987, and 1990, respectively. In 1990, he joined Fujitsu Laboratories Ltd., Atsugi, Japan, where he was engaged in the research and development of various types of semiconductor lasers. In 2003, he moved to Eudyna Devices Inc., Yamanashi, Japan, where he was working on the development of semiconductor lasers for optical communication systems as a development senior manager. In 2009, due to the organizational change of Eudyna Devices Inc., he moved to Sumitomo Electric Industries, Ltd., Yokohama, Japan, and he is now leading the development of integrated semiconductor optical devices as a department head of Transmission Devices Laboratory. Dr. Shoji is a member of IEICE, JSAP, and IEEE/Photonics Society.

Dr. Shoji is a member of IEICE, JSAP, and IEEE/Photonics Society.